JACS
JOURNAL OF THE AMERICAN CHEMICAL SOCIETY

ARTICLE

pubs.acs.org/JACS

Mesoporous Layer-by-Layer Ordered Nanohybrids of Layered Double Hydroxide and Layered Metal Oxide: Highly Active Visible Light Photocatalysts with Improved Chemical Stability

Jayavant L. Gunjakar, Tae Woo Kim, Hyo Na Kim, In Young Kim, and Seong-Ju Hwang*

Center for Intelligent Nano-Bio Materials (CINBM), Department of Chemistry and Nano Sciences, Ewha Womans University, Seoul 120-750, Korea

Supporting Information

ABSTRACT: Mesoporous layer-by-layer ordered nanohybrids highly active for visible light-induced O_2 generation are synthesized by self-assembly between oppositely charged 2D nanosheets of Zn−Cr-layered double hydroxide (Zn−Cr-LDH) and layered titanium oxide. The layer-by-layer ordering of two kinds of 2D nanosheets is evidenced by powder X-ray diffraction and cross-sectional high resolution-transmission electron microscopy. Upon the interstratification process, the original in-plane atomic arrangements and electronic structures of the component nanosheets remain intact. The obtained heterolayered nanohybrids show a strong absorption of visible light and a remarkably depressed photoluminescence signal, indicating an effective electronic coupling between the two component nanosheets. The self-assembly between 2D inorganic nanosheets leads to the formation of highly porous stacking structure, whose porosity is controllable by changing the ratio of layered titanate/Zn−Cr-LDH. The resultant heterolayered nanohybrids are fairly active for visible light-induced O_2 generation with a rate of ~1.18 mmol h^{-1} g^{-1}, which is higher than the O_2 production rate (~0.67 mmol h^{-1} g^{-1}) by the pristine Zn−Cr-LDH material, that is, one of the most effective visible light photocatalysts for O_2 production, under the same experimental condition. This result highlights an excellent functionality of the Zn−Cr-LDH−layered titanate nanohybrids as efficient visible light active photocatalysts. Of prime interest is that the chemical stability of the Zn−Cr-LDH is significantly improved upon the hybridization, a result of the protection of the LDH lattice by highly stable titanate layer. The present findings clearly demonstrate that the layer-by-layer-ordered assembly between inorganic 2D nanosheets is quite effective not only in improving the photocatalytic activity of the component semiconductors but also in synthesizing novel porous LDH-based hybrid materials with improved chemical stability.

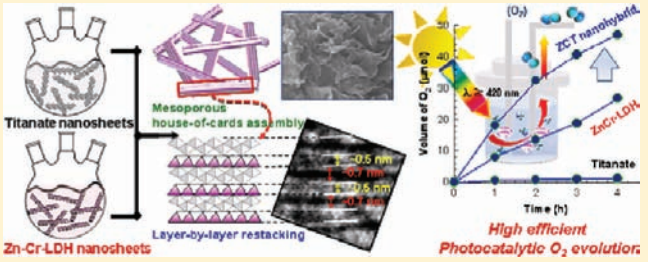

INTRODUCTION

Solar energy is one of the promising renewable energy sources that can replace fossil fuels and fulfill the rising global demand for sustainable energy. One of the most effective approaches to harvest the solar energy is the photoinduced production of H_2 and O_2 molecules by semiconductor photocatalysts.[1−6] Despite a great deal of research, most inorganic photocatalysts ever-developed are not appropriate for the visible light-induced water splitting because of their large bandgap energy, poor photostability, and unsuitable band positions for the reduction of protons and the oxidation of oxide ions.[6−8] To overcome the drawbacks of these materials, attempts are made to hybrid two kinds of photocatalysts.[9−13] In one instance, the CdS−TiO_2 hybrid system can harvest visible light with narrow bandgap CdS component, and the photogenerated electrons in CdS migrate into wide bandgap TiO_2 component. Such an electron transfer leads to the depression of electron−hole recombination and the improvement of the photocatalytic activity of CdS.[14−17] In addition to hybridization, the formation of nanostructure can provide an alternative way to enhance the photocatalytic activity of semiconducting material. Many low-dimensional nanostructured semiconducting materials are designed and explored as photocatalyst for the production of H_2 or O_2 gases.[18−22] Research interest on the nanostructured semiconductors is extended to 2D nanostructured inorganic solids. As an inorganic analogue to graphene, the subnanometer-thick 2D nanosheets of layered metal oxides can be synthesized by the soft-chemical exfoliation process of the pristine layered materials. Several exfoliated layered metal oxide nanosheets are applicable as photocatalysts for photooxidation of organic pollutant molecules and also for the photoproduction of H_2 gas.[9,12,23−31] In comparison with layered metal oxides, layered metal hydroxides such as layered double hydroxides, or LDHs, are less investigated as photocatalysts. A recent report about the high photocatalytic activity of the Zn−M-LDH (M = Cr, Ti, Al) material evokes research interest on the application of LDH phases as photocatalysts.[32−35] Taking into account the high photocatalytic efficiency and high quantum yield of the Zn−Cr-LDH

Received: April 13, 2011
Published: August 23, 2011

compound for visible light-induced O_2 generation, this material can act as a useful stepping stone for the exploration of new efficient photocatalysts. Furthermore, difficulty in the photoinduced generation of O_2 molecules that requires the involvement of four electrons raises the validity of this LDH material as useful photocatalyst. By the hybridization with other semiconductors, the photocatalytic activity of the Zn−Cr-LDH phase is expected to further increase through the increase of the lifetime of electrons and holes. Considering the 2D morphology and excellent photocatalytic activity of the layered titanate,[36,37] this material can be a useful candidate for the coupling with the LDH material. The common 2D structures of the LDH and layered titanate enable an effective physical contact and a strong electronic coupling between them. Also, the reassembling of the two sheet-like crystals is effective in enhancing the photocatalytic activity of the Zn−Cr-LDH through the formation of porous stacking structure with a large number of reaction sites.[23,36] In addition, the poor chemical stability of the Zn−Cr-LDH that frustrates the practical application of this material can be improved by the protection by highly stable layered titanate. The improvement of chemical stability is highly crucial in widening the application fields of the LDH phase. Because the exfoliated nanosheets of LDH and layered titanate possess opposite layer charges,[24−31,36−39] the layer-by-layer-ordered nanohybrids composed of two kinds of nanosheets can be synthesized by electrostatically derived self-assembly. Although various types of hybrid photocatalysts consisting of low-dimensional nanostructured materials are reported,[11−13,23−31] we are aware of no reports on the synthesis of heterolayered visible light active photocatalysts composed of intimately hybridized two kinds of inorganic 2D nanosheets.

In the present work, mesoporous layer-by-layer ordered nanohybrids with promising visible light photocatalytic activity are synthesized by electrostatically derived self-assembly between the positively charged Zn−Cr-LDH nanosheets and the negatively charged layered titanate nanosheets (the obtained nanohybrids are denoted as **ZCT**). The photocatalytic activity and chemical stability of the **ZCT** nanohybrids are investigated together with their structural and physicochemical properties.

EXPERIMENTAL SECTION

Preparation. Layered cesium titanate, $Cs_{0.67}Ti_{1.83}\square_{0.17}O_4$, and its protonated derivative, $H_{0.67}Ti_{1.83}\square_{0.17}\cdot H_2O$, were synthesized by conventional solid-state reaction and subsequent 1 M HCl treatment, respectively. The exfoliation of the layered titanate was achieved by the intercalation of tetrabutylammonium, or TBA, cations into layers of protonated titanate, as reported previously.[37] The aqueous suspension of exfoliated titanate nanosheets was freeze-dried and redispersed in formamide. The pristine Zn−Cr-LDH in the nitrate form was prepared by direct coprecipitation at room temperature as reported previously.[40] The exfoliation of Zn−Cr-LDH was achieved by vigorous shacking of LDH sample (1 g L^{-1}) in the formamide under N_2 bubbling to avoid carbonate contamination.[38] The heterolayered **ZCT** nanohybrids were synthesized by the mixing of the formamide suspensions of Zn−Cr-LDH and layered titanate nanosheets under a constant stirring at room temperature in N_2 atmosphere.[41] The restacked **ZCT** nanohybrids were restored by centrifugation at 6000 rpm, washed with formamide and absolute ethanol, and finally vacuum-dried at 65 °C for 24 h. The molar ratio of Zn−Cr-LDH to layered titanate was varied to tune the layer-by-layer restacking of the nanosheets on the basis of charge balance (1:0.91), area balance (1:1.46), and intermediate composition (1:1.16).

Characterization. The crystal structures of the Zn−Cr-LDH and **ZCT** nanohybrids were studied by powder X-ray diffraction, or XRD, using Ni-filtered Cu Kα radiations with a Rigaku diffractometer. The chemical compositions of the present compounds were analyzed with inductive coupled plasma, or ICP (Shimazu ICPS-5000), and elemental CHN analysis (CE-Instruments-EA-1110). High resolution-transmission electron microscopy/selected area-electron diffraction, or HR-TEM/SAED, analysis was done with a Jeol (JEM 2100F) microscope at an accelerating voltage of 200 kV. The nanohybrid samples embedded in epoxy resin were sliced by an ultramicrotome for the HR-TEM observation. Also, their surface morphology and elemental distribution were probed with field emission-scanning electron microscopy, or FE-SEM (Jeol JSM-6700F), equipped with energy-dispersive spectrometry, or EDS. Fourier-transform infrared (FT-IR) spectra in the frequency range of 400−4000 cm^{-1} were recorded on a Jasco FT/IR-6100 FT spectrometer. X-ray absorption near edge structure, or XANES, analyses were carried out at the beamline 7C of the Pohang Accelerator Laboratory, or PAL, in Korea. Ti K-edge, Cr K-edge, and Zn K-edge XANES data were collected at room temperature in a transmission mode using gas-ionization detectors. All of the present spectra were calibrated by simultaneously measuring the spectrum of Ti, Cr, or Zn metal foil. N_2 adsorption−desorption isotherms were measured at liquid nitrogen temperature with a gas sorption analyzer (ASAP 2020). The samples were degassed at 150 °C in a vacuum below 10^{-3} Torr for 12 h prior to measurements. Diffuse reflectance UV−vis spectra were obtained by Sinco S-4100 spectrometer equipped with an integrating sphere 60 mm in diameter using $BaSO_4$ as a standard. The photoluminescence, or PL, spectra were measured with Perkin-Elmer LS55 fluorescence spectrometer. To determine the band structure of the Zn−Cr-LDH material, CV curve was recorded with a potentiostat IVIUM STAT (Ivium Technologies, USA), using a conventional three-electrodes cell. A Pt mesh and Ag/AgCl electrode (+0.198 V vs NHE) were used as a reference and auxiliary electrode, respectively. The working electrodes were prepared by pasting a uniform layer of material with the help of Nafion binder on a glassy carbon electrode. The electrodes were immersed in 0.1 M $NaClO_4$ aqueous solution as an electrolyte under nitrogen atmosphere. For the measurement of photocatalytically produced oxygen gas, 10 mg of the nanohybrid powder was dispersed in a Pyrex reaction cell using a magnetic stirrer in 20 mL of water, and then 0.01 M $AgNO_3$ was added as a sacrificial reagent. The head space of reactor was sealed with an airtight silicon stopper, and the photocatalyst suspensions were thoroughly degassed using argon gas for 0.5 h. A 450 W Xe arc lamp (Newport) was used as a light source. Light was passed through a 10 cm IR water filter and a cutoff filter (λ > 420 nm for visible-light illumination) and then focused on the reactor. The light intensity of the oxygen evolution reactions was homogeneous up to 8 × 8 in. and was adjusted with a Si solar cell (Fraunhofer Institute for Solar Energy System; Mono-SiCKG filter; Certificate No. C-ISE269) to approximate AM 1.5 radiation (1 SUN). During the course of O_2 evolution, the reactor and total assembly were kept in Ar-flowing environment. The amount of O_2 evolved was estimated by injecting 100 μL of reactor headspace gas into online gas chromatography, or GC (Shimadzu GC-2014), after every hour. The chemical stability of Zn−Cr-LDH hybridized with layered titanate was examined by monitoring the leaching of zinc ions in the buffer solution with pH = 2, in comparison with bare Zn−Cr-LDH. After the reaction for 0.5−7 h, the concentration of zinc ions in the supernant solution was analyzed with ICP analysis.

RESULTS AND DISCUSSION

Synthesis and Exfoliation of Zn−Cr-LDH. Figure 1 represents the powder XRD patterns of the **ZCT** nanohybrids, the pristine Zn−Cr-LDH, and the protonated layered titanate. The pristine Zn−Cr-LDH material displays a series of well-developed Bragg reflections, which can be well-indexed with the hexagonal layered LDH structure having $R\bar{3}m$ rhombohedral symmetry.[42]

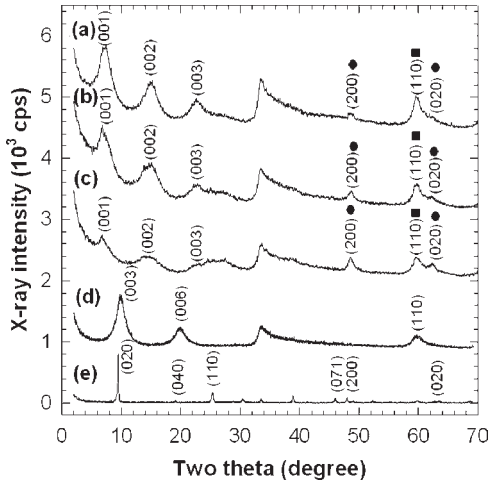

Figure 1. Powder XRD patterns of **ZCT** nanohybrids of (a) **ZCT-1**, (b) **ZCT-2**, and (c) **ZCT-3**, (d) the pristine Zn−Cr-LDH, and (e) protonated layered titanate. In the data (a−c), "●" and "■" denote in-plane Bragg reflections of exfoliated titanate nanosheets and Zn−Cr-LDH nanosheets, respectively.

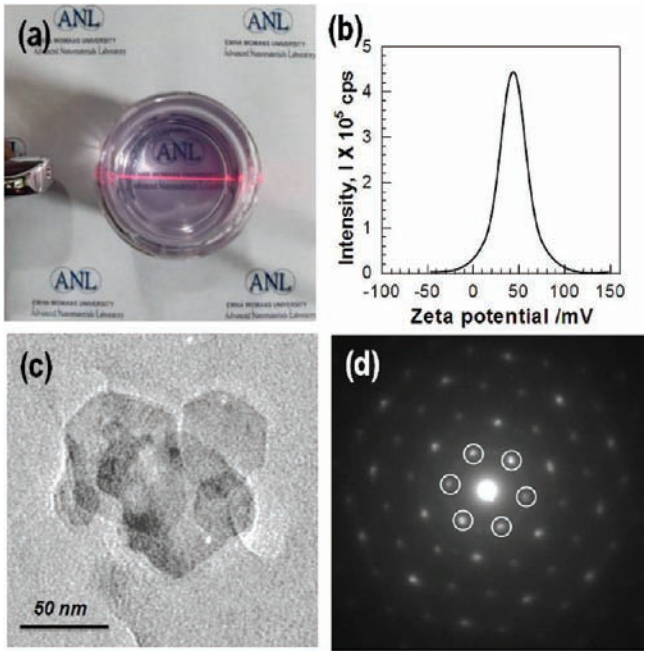

Figure 2. (a) Photoimage and (b) zeta potential curve of the colloidal suspension of exfoliated Zn−Cr-LDH nanosheet. (c) HR-TEM image and (d) SAED pattern of exfoliated Zn−Cr-LDH nanosheet.

According to the least-squares fitting analysis, the lattice parameters are determined as $a = 0.308$ nm and $c = 0.890$ nm, which is in good agreement with the lattice parameters of the nitrate-intercalated LDH phase.[32] The CHNS elemental analysis and ICP spectrometry clearly demonstrate the carbonate-free composition of the present material, that is, $Zn_{0.69}Cr_{0.31}(OH)_2 \cdot 0.31NO_3^- \cdot 0.6H_2O$. Like other LDH compounds,[38,39,43−45] the Zn−Cr-LDH material can be exfoliated into individual monolayers via dispersion of powdery samples in formamide solvent, resulting in the formation of turbid colloidal suspension. The resulting colloidal suspension of the Zn−Cr-LDH nanosheets with a light pinkish violet color is stable at room temperature for several weeks.

As illustrated in Figure 2a, the formation of the colloidal suspension of exfoliated Zn−Cr-LDH nanosheets is evidenced by the observation of a clear Tyndall phenomenon. The zeta potential measurement clearly demonstrates the positive charged state of the exfoliated Zn−Cr-LDH nanosheets; see Figure 2b. HR-TEM confirms the formation of very thin nanosheets (Figure 2c). The maintenance of the in-plane structure of LDH phase after the exfoliation is verified by SAED result in Figure 2d, in which a clear hexagonal diffraction pattern appears. The estimated in-plane lattice parameter (0.302 nm) is fairly consistent with the *a*-axis lattice parameter ($a = 0.308$ nm) determined from powder XRD analysis.

Powder XRD and HR-TEM Analyses for ZCT Nanohybrids. Three kinds of **ZCT** nanohybrids are synthesized by self-assembly between the oppositely charged nanosheets of Zn−Cr-LDH and layered titanate with the layered titanate/Zn−Cr-LDH ratios of 0.91, 1.16, and 1.46 (the obtained nanohybrids are denoted as **ZCT-1**, **ZCT-2**, and **ZCT-3**). The end ratios of 0.91 and 1.46 correspond to the compositions calculated on the basis of charge balance and area balance between two nanosheets, respectively.[46] As plotted in Figure 1, all of the present **ZCT** nanohybrids show equally spaced (00*L*) reflections in low 2θ region, indicating the layer-by-layer restacking of the nanosheets. The formation of layer-by-layer ordered structure for all of the reactant ratios adopted here strongly suggests flexibility in the chemical composition of the present hybrid materials. According to the least-squares fitting analysis, the as-prepared **ZCT** nanohybrids possess an expanded basal spacing of ∼1.22−1.31 nm, which is in good agreement with the thickness summation (∼1.2 nm) of layered titanate nanosheet and Zn−Cr-LDH nanosheet.[41] This agreement provides strong evidence for the layer-by-layer interstratification of two kinds of nanosheets. Among the present nanohybrids, the **ZCT-1** nanohybrid synthesized with the charge-balanced composition shows the strongest and sharpest (00*L*) reflections, indicating the excellent *c*-axis ordering in this compound. This finding highlights the importance of charge balance in the formation of well-ordered heterolayered materials composed of two oppositely charged nanosheets. In comparison with the **ZCT-1** nanohybrid, broader and more diffuse XRD peaks are observed for the other nanohybrids with different compositions, reflecting their poorer ordering of the component nanosheets. Such an increase of disorder in stacking structure is attributable to the incorporation of charge compensating species. On the basis of the Scherrer calculation with the full-width-at-half-maximum, or fwhm, of (00*L*) reflections, the thickness of each crystallite along the *c*-axis is estimated as ∼50−80 Å. Judging from the basal spacing of the as-prepared nanohybrids (∼12−13 Å), the obtained thickness corresponds to the ∼4−7 layers of interstratified LDH/layered titanate superlattice. As can be seen clearly from Figure 1, all of the **ZCT** nanohybrids also display several XRD peaks in high 2θ region, which correspond to the in-plane Bragg reflections of hexagonal Zn−Cr-LDH structure (denoted by "■") and to those of orthorhombic layered titanate (denoted by "●"). The observation of these in-plane reflections underscores the maintenance of the original in-plane structure of each component nanosheet after the hybridization. In addition, a broad diffraction hump appears at $2\theta = \sim 30-40°$, which is attributed to the disordered stacking structure of nanosheets.[41]

The formation of interstratified heterolayered structure of the Zn−Cr-LDH nanosheet and layered titanate nanosheet is confirmed by the HR-TEM analysis. As illustrated in Figure 3, the

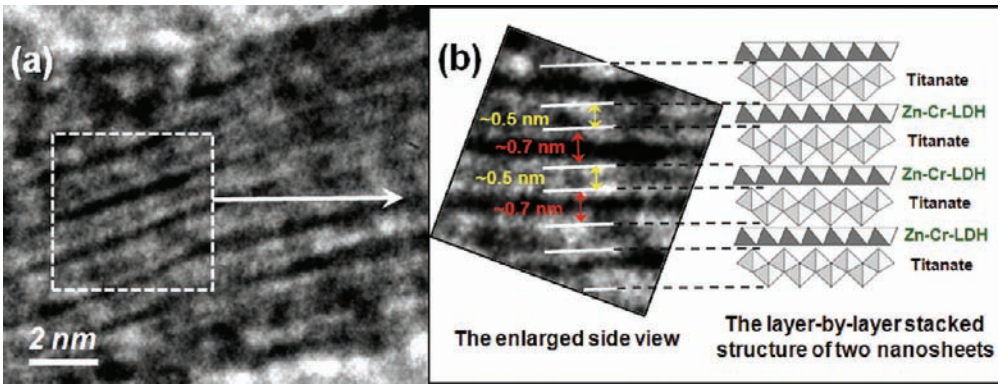

Figure 3. (a) Cross-sectional HR-TEM image of the **ZCT-1** nanohybrid and (b) its enlarged view and structural model.

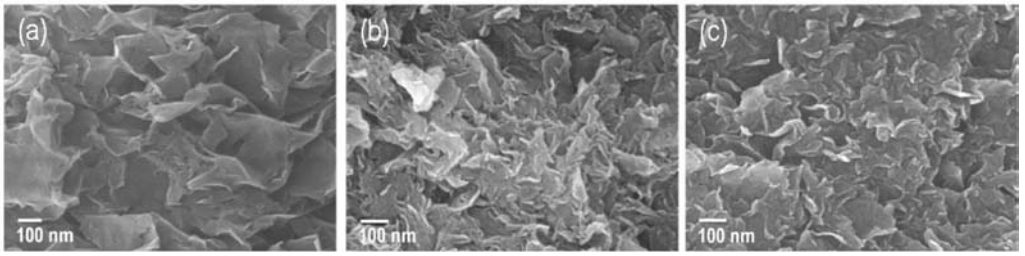

Figure 4. FE-SEM images of (a) **ZCT-1**, (b) **ZCT-2**, and (c) **ZCT-3**.

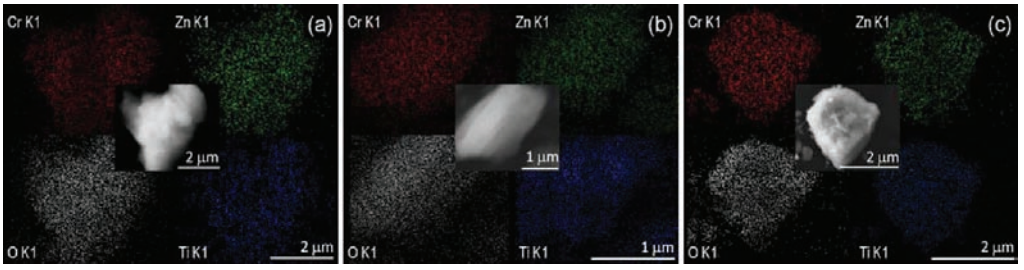

Figure 5. EDS elemental maps and (center) FE-SEM images of (a) **ZCT-1**, (b) **ZCT-2**, and (c) **ZCT-3**.

cross-sectional HR-TEM image of the **ZCT-1** nanohybrid shows parallel-aligned dark lines with two different spacings. The lattice lines with a smaller spacing of ~0.5 nm correspond to the Zn−Cr-LDH layers, whereas the other lines with a larger spacing of ~0.7 nm are assigned as the titanate layers. The observed basal spacing of the nanohybrid (~1.2 nm) is well-consistent with the *c*-axis lattice parameter determined from XRD analysis. A slight deformation of the layered lattice appears in the present image, a result of tensions caused by the use of ultramicrotome, suggesting the flexibility of the interstratified superstructures.

FE-SEM and EDS/Elemental Mapping Analyses for ZCT Nanohybrids. The morphology of the **ZCT** nanohybrids is monitored by FE-SEM analysis; see Figure 4. The images of the porous house-of-cards type stacking of sheet-like crystallites are common for all of the present nanohybrids, strongly suggesting the high porosity of these materials. A close inspection on the present FE-SEM images reveals that the particle size of the **ZCT** nanohybrids ranges from ~0.5 to ~0.8 μm, which is compatible with the size of layered titanate nanosheets (~0.45−1.0 μm) estimated from the HR-TEM and FE-SEM analysis (see the Supporting Information). This observation strongly suggests that most external surface of the porous stacking structure of the **ZCT** nanohybrid consists of layered titanate nanosheets. In comparison with the layered titanate, the HR-TEM image of the Zn−Cr-LDH nanosheet in Figure 2 indicates a smaller particle size of ~100 nm. A comparison of the particle sizes of both of the component nanosheets strongly suggests that the present **ZCT** nanohybrids possess the interstratified structure composed of smaller LDH nanoplates intercalated between the layered titanate nanosheets with larger crystal size.

To confirm the hybridization between Zn−Cr-LDH and layered titanate, the spatial distributions of metal and oxygen elements in the **ZCT** nanohybrids are examined with EDS and elemental mapping analysis. As illustrated in Figure 5, the zinc, chromium, titanium, and oxygen elements are homogeneously distributed in all of the present hybrid materials, clearly demonstrating the homogeneous mixing of two kinds of nanosheets without any spatial separation. The presence of TBA and nitrate ions in the reassembled nanohybrids is examined with FT-IR and elemental analyses (see the Supporting Information). The **ZCT-1** nanohybrid with charge-balanced formula does not exhibit distinct IR bands corresponding to nitrate and TBA ions, indicating

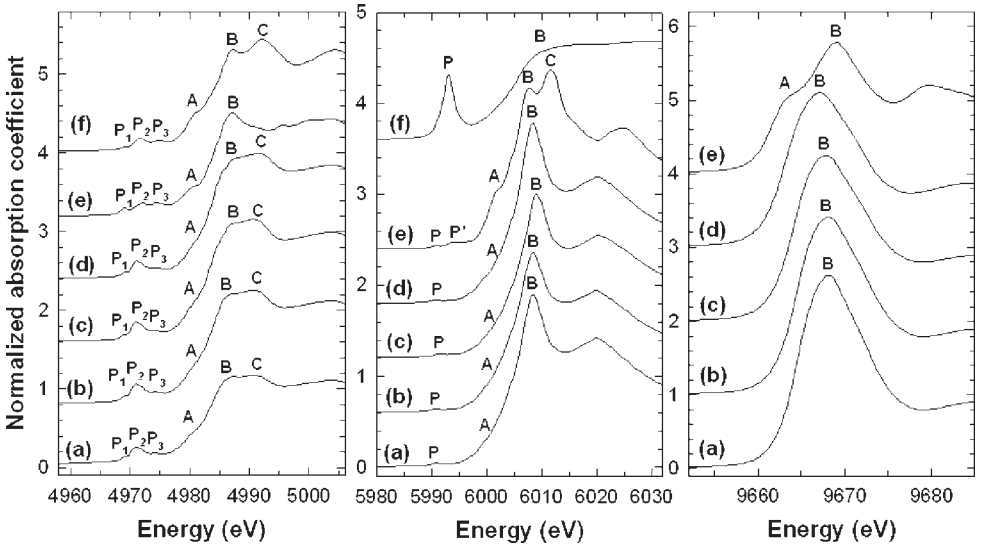

Figure 6. (Left) Ti K-edge, (middle) Cr K-edge, and (right) Zn K-edge XANES spectra of (a) **ZCT-1**, (b) **ZCT-2**, and (c) **ZCT-3**, as compared to the reference spectra of (d) the protonated layered titanate/Zn−Cr-LDH/Zn−Cr-LDH, (e) anatase TiO_2/Cr_2O_3/ZnO, and (f) rutile TiO_2/CrO_3.

the absence of these ions in this material. This observation is further confirmed by elemental analysis showing only a negligible content of nitrogen in this material. However, the other nanohybrids (**ZCT-2** and **ZCT-3**) with noncharge-balanced formula possess a much greater content of nitrogen, suggesting the presence of TBA cations. This observation can be understood in terms of the greater contents of titanate nanosheets in these two materials, in which additional TBA cations are incorporated to compensate an extra negative charge of excess layered titanate nanosheets.

An ion exchange capability of the present **ZCT** nanohybrids is also investigated. The ion-exchange reaction of the as-prepared nanohybrids with a 10-fold excess of sodium carbonate for 12 h leads to the replacement of layered titanates with carbonate ions, as evidenced by a decrease of the basal spacing of the nanohybrid. However, after a drying process at 65−150 °C, an ion exchange ability of these materials is eliminated, reflecting an increase of the lattice stability of the nanohybrid by the heat-treatment at mild temperature.

XANES Spectroscopy for ZCT Nanohybrids. The oxidation state and local symmetry of titanium, chromium, and zinc ions in the **ZCT** nanohybrids are examined with XANES analysis. The left panel of Figure 6 represents the Ti K-edge XANES spectra of the **ZCT** nanohybrids, anatase TiO_2, rutile TiO_2, and protonated layered titanate with lepidocrocite structure. All of the present materials show three pre-edge peaks (denoted as P_1, P_2, P_3) corresponding to the quadruple-allowed 1s → 3d transitions.[28,47] Overall spectral features of these pre-edge peaks provide a sensitive measure for the local crystal structure of titanium ion.[48] All of the present **ZCT** nanohybrids exhibit typical pre-edge features of lepidocrocite-structured layered titanate, which is obviously distinguishable from those of the anatase and rutile TiO_2. In the main-edge region, there are three spectral features (denoted as A, B, and C) that are assigned as the dipole-allowed 1s → 4p transitions.[47] Like the pre-edge features, the main-edge spectra of the **ZCT** nanohybrids are fairly similar to that of the lepidocrocite-type layered titanate, and not to those of rutile and anatase TiO_2 phases. The observed spectral similarity between the nanohybrids and the protonated layered titanate clearly demonstrates the maintenance of lepidocrocite-structured titanate lattice after the hybridization with the LDH nanosheets.

The Cr K-edge XANES spectra for the **ZCT** nanohybrids are compared to several reference spectra in the middle panel of Figure 6. In contrast to the reference CrO_3 compound showing a very intense pre-edge peak P, all of the **ZCT** nanohybrids as well as the pristine Zn−Cr-LDH display only a weak intensity for the pre-edge peak P corresponding to the dipole-forbidden 1s → 3d transition. This indicates the stabilization of Cr^{3+} ions in octahedral symmetry in the nanohybrid materials.[25] There are close similarities in the overall spectral feature and edge position between the **ZCT** nanohybrids and the pristine Zn−Cr-LDH, strongly suggesting the maintenance of the LDH lattice after the hybridization. The Zn K-edge XANES spectra for the **ZCT** nanohybrids are plotted in the right panel of Figure 6, together with those for the pristine Zn−Cr-LDH and bulk ZnO. The edge positions of the pristine Zn−Cr-LDH and **ZCT** nanohybrids are similar to that of reference ZnO, indicating the divalent oxidation state of Zn ions in these materials. In contrast to the reference ZnO,[49] all of the **ZCT** nanohybrids exhibit commonly poorly resolved XANES features in the energy region of 9660−9670 eV. This spectral feature is quite similar to that of the pristine Zn−Cr-LDH compound, confirming the maintenance of Zn−Cr-LDH lattice after the hybridization. The experimental findings from the Cr K-edge and Zn K-edge XANES analyses clearly demonstrate a negligible change in the crystal structure and electronic structure of the Zn−Cr-LDH component after the hybridization with layered titanate.

N_2 Adsorption−Desorption Isotherm Analysis for ZCT Nanohybrids. The surface area and pore structure of the **ZCT** nanohybrids and pristine Zn−Cr-LDH are examined with N_2 adsorption−desorption isotherm measurements. As plotted in Figure 7a, all of the present **ZCT** nanohybrids show distinct hysteresis at $pp_0^{-1} > 0.45$ and negligible N_2 adsorption at $pp_0^{-1} < 0.4$, underscoring that most porosity originates from the mesopores formed by the house-of-cards-type stacking structure of nanosheets.[28,49] This result is fairly consistent with the FE-SEM results (Figure 4). The isotherms of all of the present nanohybrids can be classified as Brunauer−Deming−Deaming−Teller,

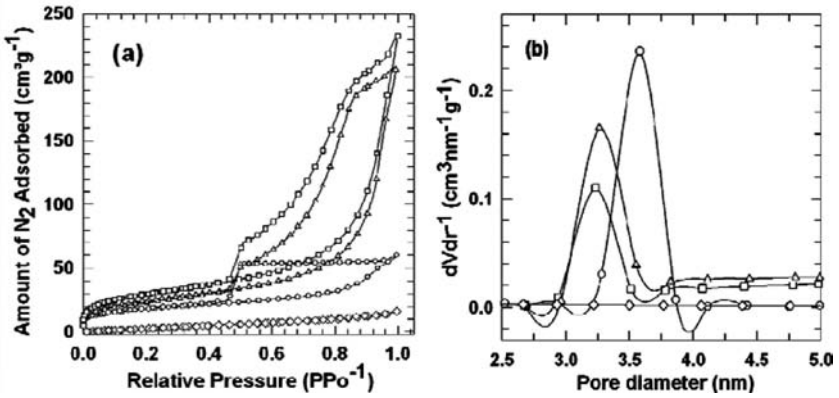

Figure 7. (a) N_2 adsorption−desorption isotherms and (b) pore size distribution curves calculated on the basis of the BJH equation for **ZCT-1** (○), **ZCT-2** (△), **ZCT-3** (□), and Zn−Cr-LDH (◇).

or BDDT, type IV shape,[50] which is characteristic of a mesoporous material having a high energy of adsorption. A distinct hysteresis loop with sloping adsorption branch and steep desorption branch at pp_0^{-1} = 0.45 is observed for the **ZCT-1** nanohybrid, which corresponds to type H2 by IUPAC classification.[51] Such a combination of type IV isotherm and type H2 hysteresis indicates the presence of well-ordered pores with narrow and wide sections and interconnecting channels.[52] Conversely, the other nanohybrids (**ZCT-2** and **ZCT-3**) exhibit type H3 hysteresis loop, showing a steep adsorption branch at high pp_0^{-1} region and a sloping desorption branch. Such a type of isotherm and hysteresis reflects open slit-shaped capillaries with parallel walls or capillaries with very wide bodies and narrow short necks, which is frequently observed for the aggregates of plate-like particles with slit-shaped pores.[50] The observed hysteresis behaviors indicate that both the **ZCT-2** and the **ZCT-3** nanohybrids have more open and less ordered pore structures than does the **ZCT-1** nanohybrid.

In contrast to the **ZCT** nanohybrids, the pristine Zn−Cr-LDH material shows only a weak adsorption of nitrogen as well as no distinct hysteresis. The observed isotherm of the pristine Zn−Cr-LDH can be classified as BDDT type-III, which is characteristic of a nonporous material.[51] According to fitting analysis based on BET equation, all of the **ZCT** nanohybrids possess markedly expanded surface areas of 67, 86, and 104 $m^2\ g^{-1}$ for **ZCT-1**, **ZCT-2**, and **ZCT-3**, respectively, whereas much smaller surface areas occur for the pristine Zn−Cr-LDH (15 $m^2\ g^{-1}$) and the pristine layered titanate (∼1 $m^2\ g^{-1}$). The observed small surface area of the Zn−Cr-LDH material is common for many other LDH phases.[53−55] Taking into account the highly anisotropic 2D morphology of LDH crystallites, the observed N_2 adsorption by the Zn−Cr-LDH material can be attributed mainly to the external planar surface of the LDH crystallites not to the edge of the LDH. Thus, the side-edge of the intercalated LDH crystallites makes only a negligible contribution to the total adsorption of nitrogen by the **ZCT** nanohybrids. As shown in Figure 7, all of the present **ZCT** nanohybrids show stronger N_2 adsorption in the higher pressure region (pp_0^{-1} > 0.45), which occurs on the external surface of mesoporous house-of-cards-type assembly of nanohybrid crystallites. The FE-SEM images in Figure 4 suggest that most external surface of the porous stacking structure of **ZCT** nanohybrids is composed of the layered titanate nanosheets. Thus, most of N_2 adsorption by the **ZCT** nanohybrids is attributable to occur on the external surface of layered titanate nanosheets.

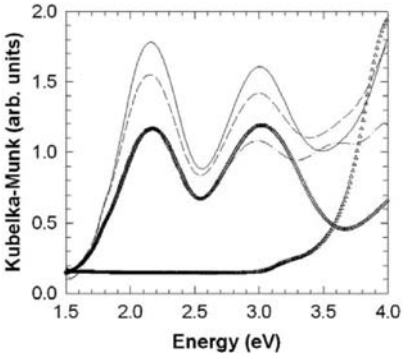

Figure 8. Diffuse reflectance UV−vis spectra (plotted as the Kubelka−Munk function of the reflectance, R) of **ZCT-1** (−), **ZCT-2** (− − −), **ZCT-3** (− · − · −), the pristine Zn−Cr-LDH (○), and the cesium titanate (△).

Among the present nanohybrids, the charge-balanced **ZCT-1** material possesses the smallest surface area. The observed dependence of surface area on the nanohybrid composition can be understood as follows: the **ZCT-1** sample synthesized with a charge-balanced ratio forms well-ordered heterolayers between the LDH and titanate nanosheets. In comparison with the **ZCT-1**, the other nanohybrids with the reactant ratios deviated from the charge-balanced composition have more porous and open structure due to the charge mismatch between two nanosheets. The pore size of the present nanohybrids is analyzed based on the Barrett−Joyner−Halenda, or BJH, method. As presented in Figure 7b, in contrast to the pristine Zn−Cr-LDH having no mesopore, all of the **ZCT** nanohybrids have mesopores with the average diameter of ∼3.3−3.9 nm. Judging from the pore size and basal spacing of the nanohybrids, the observed mesopores should originate from the stacking structure of nanohybrid crystallites.

Diffuse Reflectance UV−Vis and PL Spectroscopy and Band Structure Determination of ZCT Nanohybrids. The electronic structure and optical property of the **ZCT** nanohybrids are probed with diffuse reflectance UV−vis spectroscopy. As plotted in Figure 8, the pristine Zn−Cr-LDH material shows two strong absorption peaks at 2.2 and 3.0 eV corresponding to the d−d transitions of trivalent chromium ions.[32] Upon the hybridization with the Zn−Cr-LDH, the resulting nanohybrid materials commonly display strong absorption of visible radiation with two absorption features, indicating an effective electronic

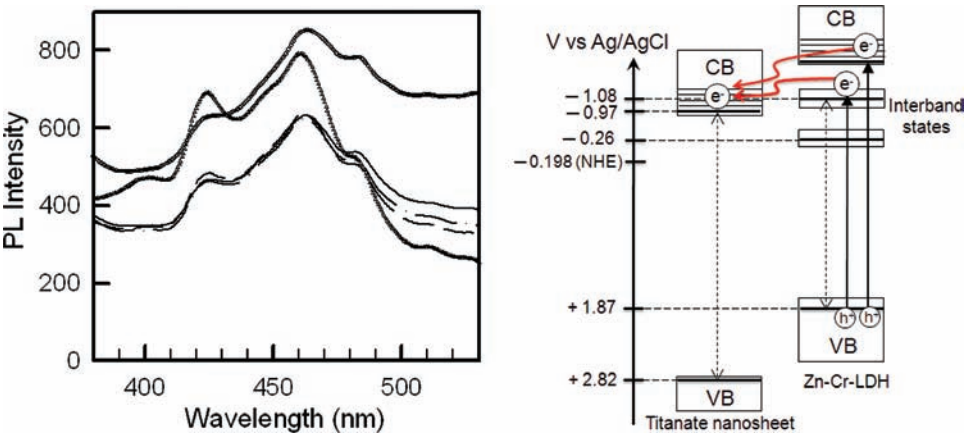

Figure 9. (Left) PL spectra of **ZCT-1** (—), **ZCT-2** (– – –), **ZCT-3** (— · — · —), the pristine Zn—Cr-LDH (○), and protonated layered titanate (△). (Right) Schematic model for the band structures of **ZCT** nanohybrid.

coupling between layered titanate and the Zn—Cr-LDH nanosheets. The observed strong absorption of visible light suggests the possible functionality of the **ZCT** nanohybrids as visible light active photocatalyst.

The change of PL signal upon the hybridization is monitored to probe an electron transfer between Zn—Cr-LDH and layered titanate. As presented in the left panel of Figure 9, the PL signal of the pristine Zn—Cr-LDH becomes significantly weaker after the hybridization with layered titanate, indicating the notable depression of the electron—hole recombination. Also, the observed PL intensities of all of the **ZCT** nanohybrids are much weaker than that of the pristine layered titanate, confirming the decrease of electron—hole recombination rate upon hybridization. This phenomenon can be ascribed to an electron transfer between Zn—Cr-LDH and layered titanate, leading to the spatial separation of electrons and holes. The resultant depression of electron—hole recombination is surely advantageous for the improvement of the photocatalytic activity.

To understand an electron transfer between Zn—Cr-LDH and layered titanate, the band structure of the Zn—Cr-LDH is estimated from the results of electrochemical CV measurement and UV—vis spectroscopy. The position of the lowest unoccupied interband state causing the first absorption peak at ~2.2 eV in the UV—vis spectrum of Zn—Cr-LDH can be determined by the on-set potential of reduction peak in the CV data.[56] As illustrated in the right panel of Figure 9, the Zn—Cr-LDH compound shows higher positions for the upper interband state corresponding to the absorption peak at ~3.0 eV in the UV—vis spectrum as well as the conduction band, or CB, in comparison with the CB of the layered titanate component.[57] The photogenerated electrons in the Zn—Cr-LDH can migrate into the CB of the layered titanate, leading to the spatial separation of electrons and holes. The resulting depression of electron—hole recombination is responsible for the observed decrease of PL intensity after the hybridization.

Photocatalytic Activity Tests for ZCT Nanohybrids. The photocatalytic activity of the **ZCT** nanohybrids is investigated by monitoring the time-dependent O_2 generation under visible illumination (λ > 420 nm). To clearly demonstrate the effect of hybridization on the photocatalytic activity, the O_2 production by the pristine Zn—Cr-LDH and layered titanate is also examined. As plotted in the left panel of Figure 10, the pristine Zn—Cr-LDH material is highly active for the visible light-induced O_2 generation, which is consistent with a recent report on this phase.[32] Conversely, the layered titanate is photocatalytically inactive in the given condition because of its wide bandgap nature. After the hybridization with layered titanate, the high photocatalytic activity of the Zn—Cr-LDH material is remarkably enhanced for all of the present ratios of layered titanate/Zn—Cr-LDH. Although the hybridization with layered titanate decreases the content of Zn—Cr-LDH phase in the final products, the O_2 generation rate of the **ZCT-1** nanohybrid (1.18 mmol h^{-1} g^{-1}) is almost twice as high as the pristine Zn—Cr-LDH (0.67 mmol h^{-1} g^{-1}).[32] Because of significant differences between experimental conditions adopted in the present study and in previous literatures, it is quite difficult to directly compare the photocatalytic activity of the present **ZCT** nanohybrids with those of other efficient photocatalysts ever-reported. However, taking into account the fact that the pristine Zn—Cr-LDH phase is one of the most effective photocatalysts for visible light-induced O_2 generation,[32] the present **ZCT** nanohybrids with further improved photocatalytic activity can be regarded as highly efficient visible light photocatalysts for photoinduced O_2 production. To examine the stability of the photocatalytic activity of the **ZCT** nanohybrid, the photocatalytic performance of **ZCT-1** nanohybrid is examined with repeated photoreactions for three cycles. The present **ZCT-1** nanohybrid retains its photocatalytic activity with only a slight decrease for consecutive three cycles (see the Supporting Information), clearly demonstrating the highly stable photocatalytic activity of the present nanohybrid material. Such a minute degrading of the photocatalytic activity is also reported for the pure Zn—Cr-LDH material and interpreted as a result of Ag deposition on the surface catalytic sites of photocatalyst.[32] To probe the possible deposition of silver metal as well as to examine the effect of photoreaction on the crystal structure, crystal morphology, and chemical composition of the **ZCT** nanohybrid, diffraction and microscopic analyses are carried out for the **ZCT-1** nanohybrid restored from the photoreactor (see the Supporting Information). The powder XRD and FE-SEM data of the restored **ZCT** nanohybrid clearly demonstrate the maintenance of its original interstratified structure and mesoporous stacking morphology after the repeated photoreactions, underscoring the high stability of this nanohybrid material. In addition, the deposition of silver metal on the surface of the nanohybrid material from the reduction of $AgNO_3$ is obviously evidenced by the results of XRD and EDS analyses. This is responsible for the observed slight decrease of

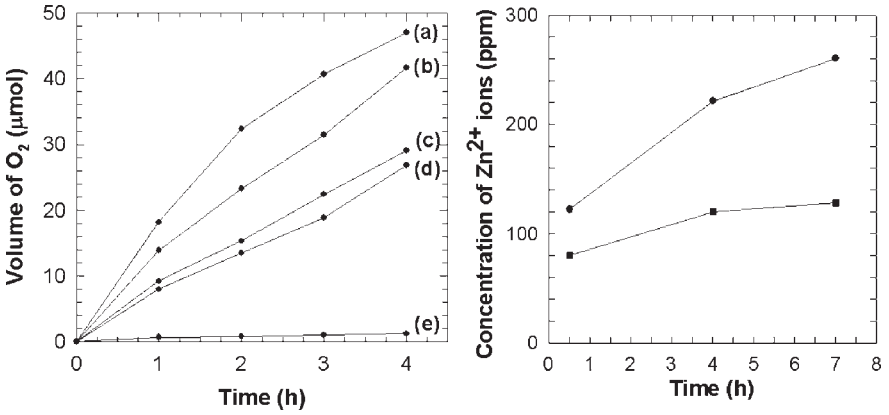

Figure 10. (Left) Time-dependent photoproduction of oxygen gas under visible light illumination ($\lambda > 420$ nm) by (a) **ZCT-1**, (b) **ZCT-2**, and (c) **ZCT-3**, as compared to the data by (d) the pristine Zn−Cr-LDH and (e) layered cesium titanate. 10 mmol of $AgNO_3$ is used as an electron scavenger. (Right) Time-dependent variation of zinc concentration dissolved from the **ZCT-1** nanohybrid (■) and the pristine Zn−Cr-LDH (●).

the photocatalytic activity of the nanohybrid during the repeated photocatalyst tests.

To further verify the positive effect of the hybridization of layered titanate on the photocatalytic activity of Zn−Cr-LDH, two kinds of control experiments are carried out (see the Supporting Information). First, the photocatalyst tests are performed for the physical mixture of Zn−Cr-LDH and layered cesium titanate and for the physical mixture of Zn−Cr-LDH and layered protonated titanate. Both of the physical mixtures show much lower photocatalytic activity for the visible light-induced O_2 evolution than the **ZCT-1** nanohybrid, underscoring the advantages of nanoscale hybridization between intimately coupled nanosheets. Second, a hybrid material composed of Zn−Cr-LDH nanosheets and TiO_2 nanoparticles is prepared to compare its photocatalytic activity with the **ZCT-1** nanohybrid. This hybrid material is less active for the visible light-induced O_2 generation than the **ZCT-1** nanohybrid composed of Zn−Cr-LDH and layered titanate nanosheets, clearly demonstrating the advantage of layered titanate nanosheets in improving the photocatalytic activity of the LDH through hybridization. The improvement of the photocatalytic activity of the Zn−Cr-LDH after the hybridization with layered titanate nanosheets can be attributed to an electronic coupling between two semiconducting nanosheets and also to the expansion of surface area. As evidenced by the results of PL and band structure determination (Figure 9), the electronic coupling between layered titanate and Zn−Cr-LDH causes the spatial separation of photoinduced holes and electrons, leading to the depression of electron−hole recombination. Also, the surface expansion upon hybridization can make additional contribution to the improvement of photocatalytic activity through the provision of more reaction sites. Among the present nanohybrids, the **ZCT-1** nanohybrid with smaller surface area is more photocatalytically active than the other nanohybrids. Such a higher performance of this material can be ascribed not only to its higher content of Zn−Cr-LDH nanosheets but also to its more ordered hybrid structure, resulting in the more facile movement of holes to reaction sites and an effective electron−hole separation.

In addition, the photocatalytic activity of the **ZCT** nanohybrid is tested for visible light-induced evolution of H_2 gas (see the Supporting Information). The Pt-loaded **ZCT-1** nanohybrid can induce H_2 evolution under the irradiation of visible light ($\lambda \geq 420$ nm) with the sacrificial agent of 0.1 M methanol solution. Yet the observed activity for H_2 production is not very high. As plotted in the UV−vis spectra (Figure 8), visible light irradiated on the **ZCT** nanohybrid is absorbed mainly by the Zn−Cr-LDH component, but this material is known to be almost inactive for H_2 production.[32] Thus, the low photocatalytic activity of Zn−Cr-LDH component for H_2 production would be the reason for the observed low performance of the **ZCT** nanohybrid for the same photoreaction.

Chemical Stability Tests for ZCT Nanohybrid. The effect of hybridization with layered titanate on the chemical stability of the Zn−Cr-LDH is tested by monitoring the time-dependent dissolution of zinc ions from the **ZCT-1** nanohybrid and the pristine Zn−Cr-LDH in acidic media; see the right panel of Figure 10. For the stability tests, 0.019 g of Zn−Cr-LDH is reacted with 20 mL of acidic buffer solution with pH = 2, whereas 0.03 g of the **ZCT** nanohybrid containing the same amount of Zn ions is used. In comparison with the bare Zn−Cr-LDH showing significant leaching of Zn ions, the **ZCT-1** nanohybrid displays less prominent dissolution of Zn ions. Because of the presence of surface-exposed Zn−Cr-LDH, the **ZCT** nanohybrid shows notable dissolution of Zn ions at the initial stage of stability test. Yet as the reaction proceeds, the leaching of Zn ions from the **ZCT** nanohybrid is significantly depressed, resulting in greater solubility difference between the nanohybrid and the pristine LDH material. The effect of chemical etching on the crystal structure, morphology, and chemical composition of the **ZCT-1** nanohybrid is monitored by powder XRD, FE-SEM, and EDS elemental mapping analyses (see the Supporting Information). After the chemical etching test, the restored **ZCT-1** nanohybrid shows the original diffraction peak of interstratified structure, confirming the maintenance of original nanohybrid structure. The FE-SEM image of the restored nanohybrid material clearly demonstrates the retention of the house-of-cards-type stacking structure, underscoring no significant effect of acid etching on the morphology of the **ZCT** nanohybrid. Also, the EDS analysis provides clear evidence for the coexistence of Zn−Cr-LDH and layered titanate nanosheets in the etched **ZCT** nanohybrid. All of the results presented here provide strong evidence for the significant improvement of the chemical stability of the Zn−Cr-LDH by the protection of highly stable titanate layers. Considering that the poor stability of Zn−Cr-LDH phase prohibits the use of this photocatalyst material in acidic media, the formation of heterolayered nanohybrid with layered titanate can provide a highly useful way to widen the application fields of the LDH material.

CONCLUSION

Layer-by-layer ordering of positively charged Zn−Cr-LDH 2D nanosheets and negatively charged layered titanate 2D nanosheets yields mesoporous heterolayered **ZCT** nanohybrids with an excellent photocatalytic activity for visible light-induced O_2 generation and an improved chemical stability. The resultant heterolayered nanohybrids possess a visible light harvesting ability and a highly porous structure, which are attributable to the electronic coupling between the component nanosheets and the house-of-cards-type stacking of the layered crystallites, respectively. As a result of the protection of the LDH lattice by layered titanate, the chemical stability of the Zn−Cr-LDH is significantly improved. Regardless of chemical composition, the **ZCT** nanohybrids show highly efficient photocatalytic activity for O_2 production under visible illumination, which is superior to the activities of the pristine Zn−Cr-LDH and layered titanate. The ordering of heterolayered materials is fairly important in optimizing visible light-induced photocatalytic activity of component nanosheet. Such a well-ordered heterolayer structure can be fabricated by hybridization between two oppositely charged nanosheets with the charge-balanced composition. Considering that the pristine Zn−Cr-LDH phase is one of the most efficient visible light photocatalysts,[32] the present **ZCT** nanohybrids with further improved photocatalytic activity must be one of the best photocatalyst materials applicable for visible light-induced O_2 production. The present experimental results highlight the usefulness of the hybridization between cationic and anionic inorganic 2D nanosheets in developing highly efficient visible light active photocatalysts with improved chemical stability. Our current project is the application of the present synthetic strategy to other couples of anionic nanosheets like graphene, layered metal oxides, layered metal phosphates, aluminosilicate clay, and cationic LDH nanosheets to synthesize novel heterolayered nanohybrid materials with improved functionalities as catalysts, electrodes, adsorbents, etc.

ASSOCIATED CONTENT

Supporting Information. FE-SEM and HR-TEM images of the exfoliated titanate nanosheets. FT-IR spectra of Zn−Cr-LDH, freeze-dried titanate nanosheets, and **ZCT** nanohybrid. Photocatalytic activity plots of the **ZCT** nanohybrid (for repeated O_2 evolution and H_2 evolution), the physical mixtures of Zn−Cr-LDH and layered titanium oxides, and the hybrid material of Zn−Cr-LDH nanosheets and TiO_2 nanoparticles. Powder XRD pattern and FE-SEM/EDS data of the **ZCT** nanohybrids after the repeated photocatalyst tests and chemical etching tests. This material is available free of charge via the Internet at http://pubs.acs.org.

AUTHOR INFORMATION

Corresponding Author
hwangsju@ewha.ac.kr

ACKNOWLEDGMENT

This research is supported by the Korea Ministry of Environment as "Converging Technology Project" (191-101-001) and by a National Research Foundation of Korea Grant funded by the Korean Government (2010-0001485). The experiments at PAL were supported in part by MOST and POSTECH.

REFERENCES

(1) Fujishima, A.; Honda, K. *Nature* **1972**, *238*, 37–38.
(2) Zou, Z.; Ye, J.; Sayama, K.; Arakawa, H. *Nature* **2001**, *414*, 625–627.
(3) Kato, H.; Asakura, K.; Kudo, A. *J. Am. Chem. Soc.* **2003**, *125*, 3082–3089.
(4) Lewis, N. S.; Nocera, D. G. *Proc. Natl. Acad. Sci. U.S.A.* **2006**, *103*, 15729–15735.
(5) Chen, X.; Shen, S.; Guo, L.; Mao, S. S. *Chem. Rev.* **2010**, *110*, 6503–6570.
(6) Kudo, A.; Miseki, Y. *Chem. Soc. Rev.* **2009**, *38*, 253–278.
(7) Kudo, A. *Int. J. Hydrogen Energy* **2007**, *32*, 2673–2678.
(8) Lewis, N. S. *Nature* **2001**, *414*, 589–590.
(9) Shangguan, W. F. *Sci. Technol. Adv. Mater.* **2007**, *8*, 76–81.
(10) Zhang, L. L.; Zhang, W. G.; Lu, L. D.; Yang, X. J.; Wang, X. *J. Mater. Sci.* **2006**, *41*, 3917–3921.
(11) Maeda, K.; Higashi, M.; Lu, D.; Abe, R.; Domen, K. *J. Am. Chem. Soc.* **2010**, *132*, 5858–5868.
(12) Kim, T. W.; Ha, H. W.; Paek, M. J.; Hyun, S. H.; Baek, I. H.; Choy, J.-H.; Hwang, S.-J. *J. Phys. Chem. C* **2008**, *112*, 14853–14862.
(13) Kim, T. W.; Hwang, S.-J.; Jhung, S. H.; Chang, J. S.; Park, H.; Choi, W.; Choy, J.-H. *Adv. Mater.* **2008**, *20*, 539–542.
(14) Hirai, T.; Okubo, H.; Komasawa, I. *J. Colloid Interface Sci.* **2001**, *235*, 358–364.
(15) Wu, J. H.; Lin, J. M.; Shu, Y. B.; Sato, T. *J. Mater. Chem.* **2001**, *11*, 3343–3347.
(16) Shangguan, W. F.; Yoshida, A. *Sol. Energy Mater. Sol. Cells* **2001**, *69*, 189–194.
(17) Shangguan, W. F.; Yoshida, A. *J. Phys. Chem. B* **2002**, *106*, 12227–12230.
(18) Jing, D. W.; Guo, L. J. *J. Phys. Chem. C* **2007**, *111*, 13437–13441.
(19) Lee, Y. L.; Chi, C. F.; Liau, S. Y. *Chem. Mater.* **2010**, *22*, 922–927.
(20) Navarro, R. M.; del Valle, F.; Fierro, J. L. G. *Int. J. Hydrogen Energy* **2008**, *33*, 4265–4273.
(21) Lin, Y.; Zhou, S.; Sheehan, W. S.; Wang, D. *J. Am. Chem. Soc.* **2011**, *133*, 2398–2401.
(22) Hara, M.; Takata, T.; Kondo, J. N.; Domen, K. *Catal. Today* **2004**, *90*, 313–317.
(23) Kim, T. W.; Hur, S. G.; Hwang, S.-J.; Park, H.; Choi, W.; Choy, J.-H. *Adv. Funct. Mater.* **2007**, *17*, 307–314.
(24) Tagusagawa, C.; Takagaki, A.; Hayashi, S.; Domen, K. *J. Am. Chem. Soc.* **2008**, *130*, 7230–7231.
(25) Jang, J. S.; Kim, H. G.; Reddy, V. R.; Bae, S. W.; Ji, S. M.; Lee, J. S. *J. Catal.* **2005**, *231*, 213–222.
(26) Choy, J.-H.; Lee, H. C.; Jung, H.; Kim, H.; Boo, H. *Chem. Mater.* **2002**, *14*, 2486–2491.
(27) Fujishiro, Y.; Uchida, S.; Sato, T. *Int. J. Inorg. Mater.* **1999**, *1*, 67–72.
(28) Kim, T. W.; Hwang, S.-J.; Park, Y.; Choi, W.; Choy, J.-H. *J. Phys. Chem. C* **2007**, *111*, 1658–1664.
(29) Paek, M. J.; Kim, T. W.; Hwang, S.-J. *J. Phys. Chem. Solids* **2008**, *69*, 1444–1446.
(30) Shibata, T.; Sakai, N.; Fukuda, K.; Ebina, Y.; Sasaki, T. *Phys. Chem. Chem. Phys.* **2007**, *9*, 2413–2420.
(31) Ebina, Y.; Sakai, N.; Sasaki, T. *J. Phys. Chem. B* **2005**, *109*, 17212–17216.
(32) Gomes Silva, C.; Bouizi, Y.; Fornes, V.; Garcia, H. *J. Am. Chem. Soc.* **2009**, *131*, 13833–13839.
(33) Lee, Y.; Choi, J. H.; Jeon, H. J.; Choi, K. M.; Lee, J. W.; Kang, J. K. *Energy Environ. Sci.* **2011**, *4*, 914–920.
(34) Zhao, Y.; Wei, M.; Lu, J.; Wang, Z. L.; Duan, X. *ACS Nano* **2009**, *3*, 4009–4016.
(35) Wang, H.; Xiang, X.; Li, F. *AIChE J.* **2010**, *56*, 668–678.
(36) Choy, J.-H.; Lee, H. C.; Jung, H.; Hwang, S.-J. *J. Mater. Chem.* **2001**, *11*, 2232–2234.
(37) Sasaki, T.; Watanabe, M. *J. Am. Chem. Soc.* **1998**, *120*, 4682–4689.
(38) Li, L.; Ma, R. Z.; Ebina, Y.; Iyi, N.; Sasaki, T. *Chem. Mater.* **2005**, *17*, 4386–4391.

(39) Ma, R. Z.; Liu, Z. P.; Li, L.; Iyi, N.; Sasaki, T. *J. Mater. Chem.* **2006**, *16*, 3809–3813.
(40) Prevot, V.; Forano, C.; Besse, J. P. *Inorg. Chem.* **1998**, *37*, 4293–4301.
(41) Li, L.; Ma, R. Z.; Ebina, Y.; Fukuda, K.; Takada, K.; Sasaki, T. *J. Am. Chem. Soc.* **2007**, *129*, 8000–8007.
(42) Taviot-Gueho, C.; Leroux, F.; Payen, C.; Besse, J. P. *Appl. Clay Sci.* **2005**, *28*, 111–120.
(43) Ma, R. Z.; Liu, Z. P.; Takada, K.; Iyi, N.; Bando, Y.; Sasaki, T. *J. Am. Chem. Soc.* **2007**, *129*, 5257–5263.
(44) Ma, R.; Takada, K.; Fukuda, K.; Iyi, N.; Bando, Y.; Sasaki, T. *Angew. Chem., Int. Ed.* **2008**, *47*, 86–89.
(45) Liu, Z. P.; Ma, R. Z.; Osada, M.; Iyi, N.; Ebina, Y.; Takada, K.; Sasaki, T. *J. Am. Chem. Soc.* **2006**, *128*, 4872–4880.
(46) The in-plane lattice parameters of titanate nanosheets with orthorhombic symmetry are a = 0.3760 and c = 0.2976 nm, and thus its 2D unit cell area is calculated as 0.112 nm^2. This in-plane unit cell contains two formula units of TiO_x with a net negative charge of −0.68. The 2D unit cell area of hexagonal $Zn_{0.69}Cr_{0.31}(OH)_2$ nanosheet is 0.082 nm^2 (0.308 × 0.308 × sin 120°). A single formula unit of LDH possesses a net positive charge of +0.31. From these data, the molar ratio of layered titanate/$Zn_{0.69}Cr_{0.31}(OH)_2$ is calculated as 0.91 and 1.46 for the charge-balanced composition and area-balanced composition, respectively.
(47) Hur, S. G.; Park, D. H.; Kim, T. W.; Hwang, S.-J. *Appl. Phys. Lett.* **2004**, *85*, 4130–4132.
(48) Paek, M. J.; Ha, H. W.; Kim, T. W.; Moon, S. J.; Baeg, J. O.; Choy, J.-H.; Hwang, S.-J. *J. Phys. Chem. C* **2008**, *112*, 15969–15972.
(49) Kim, T. W.; Hur, S. G.; Hwang, S.-J.; Choy, J.-H. *Chem. Commun.* **2006**, 220–222.
(50) Condon, J. B. *Surface Area and Porosity Determinations by Physisorption: Measurements and Theory*, 1st ed.; Elsevier: Amsterdam; Boston, 2006; p 274.
(51) Allen, T. *Powder Sampling and Particle Size Determination*, 1st ed.; Elsevier: Amsterdam; Boston, 2003; p 660.
(52) Gregg, S. J.; Sing, K. S. W. *Adsorption, Surface Area, and Porosity*, 2nd ed.; Academic Press: London; New York, 1982; p 303.
(53) Beaudot, P.; De Roy, M.; Besse, J. *Chem. Mater.* **2004**, *16*, 935–945.
(54) Bouhent, M.; Derriche, Z.; Denoyel, R.; Prevot, V.; Forano, C. *J. Solid State Chem.* **2011**, *184*, 1016–1024.
(55) Carriazo, D.; Domingo, C.; Martin, C.; Rives, V. *Inorg. Chem.* **2006**, *45*, 1243–1251.
(56) Saruwatari, K.; Sato, H.; Idei, T.; Kameda, J.; Yamagishi, A.; Takagaki, A.; Domen, K. *J. Phys. Chem. B* **2005**, *109*, 12410–12416.
(57) Sakai, N.; Ebina, Y.; Takada, K.; Sasaki, T. *J. Phys. Chem. B* **2005**, *109*, 9651–9655.